Single-mode, low loss hollow-core antiresonant fiber designs

Habib, Md Selim; Antonio-Lopez, J. E.; Markos, Christos; Schülzgen, Axel; Amezcua-Correa, Rodrigo

Published in:
Optics Express

Link to article, DOI:
10.1364/OE.27.003824

Publication date:
2019

Document Version
Publisher's PDF, also known as Version of record

Research Article | Vol. 27, No. 4 | 18 Feb 2019 | OPTICS EXPRESS 3824
Optics EXPRESS

Single-mode, low loss hollow-core anti-resonant fiber designs

MD. SELIM HABIB,[1,*] J. E. ANTONIO-LOPEZ,[1] CHRISTOS MARKOS,[2] AXEL SCHÜLZGEN,[1] AND RODRIGO AMEZCUA-CORREA[1]

[1]*CREOL, The College of Optics and Photonics, University of Central Florida, Orlando, FL-32816, USA*
[2]*DTU Fotonik, Technical University of Denmark, DK-2800, Denmark*
[*]*mdselim.habib@creol.ucf.edu*

Abstract: In this paper, we numerically investigate various hollow-core anti-resonant (HC-AR) fibers towards low propagation and bend loss with effectively single-mode operation in the telecommunications window. We demonstrate how the propagation loss and higher-order mode modal contents are strongly influenced by the geometrical structure and the number of the anti-resonant cladding tubes. We found that 5-tube nested HC-AR fiber has a wider anti-resonant band, lower loss, and larger higher-order mode extinction ratio than designs with 6 or more anti-resonant tubes. A loss ratio between the higher-order modes and fundamental mode, as high as 12,000, is obtained in a 5-tube nested HC-AR fiber. To the best of our knowledge, this is the largest higher-order mode extinction ratio demonstrated in a hollow-core fiber at 1.55 μm. In addition, we propose a modified 5-tube nested HC-AR fiber, with propagation loss below 1 dB/km from 1330 to 1660 nm. This fiber also has a small bend loss of ~15 dB/km for a bend radius of 1 cm.

1. Introduction

Hollow-core fibers have been extensively studied and fabricated by several research groups around the globe over the past two decades due to their extraordinary ability of light guidance in an air-core [1–9]. A unique and striking feature of hollow-core fiber is that most of the light (>99.99%) can be guided in the central air-core with only a tiny fraction of light overlapping with the surrounding glass structure, hence increasing the optical damage threshold and reducing material absorption significantly [4–6,10,11]. These fibers have found numerous applications including high power delivery [12], ultra-short pulse delivery [13], pulse compression [14], mid-infrared (mid-IR) transmission [15], terahertz guidance [16], and gas-based nonlinear optics [17–25]. In general, based on the guidance mechanism, there are two types of hollow-core fibers which have been proposed. In the first type, hollow-core photonic bandgap (HC-PBG) fiber, light is guided inside the air-core via PBG effect [1]. In these fibers, the cladding does not support modes for certain ranges of optical wavelengths and propagation constants modes thus confining the light with low loss. The lowest experimental loss value of a HC-PBG fiber is 1.7 dB/km at 1.62 μm with a transmission band of 70 nm [26], which is limited by surface modes [27] and surface scattering loss (SSL) [28]. In addition to their limited transmission bandwidth, HC-PBG fibers exhibit rather large power overlap of the core modes with the glass cladding and high group-velocity dispersion (especially close to the band-gap edges) [29].

The other class of hollow-core fiber is typically referred to as “inhibited coupling” fibers. In these structures, light guidance is supported via inhibited coupling between the core guided modes and a continuum of cladding modes [30,31]. Recently, these fibers have sparked great interest owing to its remarkable transmission properties such as broad bandwidth, very low power overlap with the glass regions, low dispersion, and low loss levels. Kagome fiber, a design first demonstrated by Benabid *et al*. [3], is an example of inhibited coupling fibers. Numerical and experimental investigations suggested that the core contour plays a crucial role

#344492 https://doi.org/10.1364/OE.27.003824
Journal © 2019 Received 11 Sep 2018; revised 27 Dec 2018; accepted 31 Dec 2018; published 4 Feb 2019

Optics EXPRESS

on the fiber modal properties [32–34]. In this regard, an optimized Kagome fiber with a hypocycloid-shape has been already demonstrated with loss as low as 13.9 dB/km at 1.55 μm [35]. On the other hand, negative curvature hollow-core anti-resonant (HC-AR) fibers are another type of "inhibited coupling" fibers which have gained significant attention over the past few years due to their potential for achieving ultra-low loss [36–38]. Contrarily to HC-PBGs, surface modes can easily be suppressed in HC-AR fibers [32] and, thus, SSL can be reduced by one order of magnitude [6,29]. In order to control the modal content and attenuation, several types of HC-AR fibers have been proposed, investigated, and fabricated, including HC-AR fibers with circular anti-resonant tubes [4,10,38–41], "ice-cream cone" shape anti-resonant tubes [41,42], elliptical anti-resonant tubes [43], nested anti-resonant tubes [5,6,11], as well as cladding tubes with even more complex shapes [44]. Recently, Debord *et al*. [38] demonstrated a single ring HC-AR fiber with 8 non-touching circular tubes with a propagation loss of 7.7 dB/km at 750 nm and a bend loss of 0.03 dB/turn at a bend radius of 15 cm. Although these are impressive numbers, such loss levels are still not sufficient to compete with the telecommunication standard [36]. Importantly, this particular 8-capillary design does not provide effectively single-mode operation [38]. On the other hand, very recently Gao *et al*. [36,37] proposed and manufactured a conjoined HC-AR fiber with loss of 2 dB/km, low bend loss, and effectively single-mode performance.

Here we systematically study different HC-AR fiber structures with the objective to identify bend insensitive designs with propagation loss <1 dB/km and single-mode operation at telecommunication wavelengths. In order to get full information on modal contents of the fibers, we investigate the propagation losses of the fundamental mode (FM) and higher-order modes (HOMs) as a function of the cladding parameters. Our numerical investigations predict that a proper selection of the number of the cladding anti-resonant tubes and the cladding geometry is crucial for minimizing propagation loss and for effectively single-mode operation.

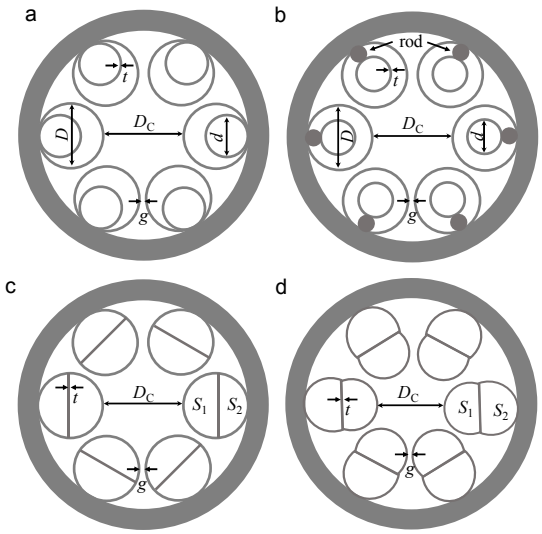

Fig. 1. Geometries considered in the calculations. (a) Typical nested HC-AR fiber; (b) modified nested HC-AR fiber with 1 supporting rod; (c) HC-AR fiber with a straight glass bar at the center of the cladding tubes; and (d) conjoined HC-AR. All fibers have the same core diameter D_c = 30.5 μm, a uniform silica wall thickness t = 1120 nm, and the same gap separation g = 6.50 μm. The diameter of the inner nested tubes d is defined by $d = D/2$ for fibers shown in (a) and (b), respectively. The areas of the D-shaped tubes are $S_1 \simeq 730$ μm^2 and $S_2 \simeq 730$ μm^2 for the fiber in (c) and S_1 = 270 μm^{2}and S_2 = 335 μm^2 for the fiber in (d), respectively.

Optics EXPRESS

2. Fiber geometry

Figure 1 shows 6-tube HC-AR fibers with different cladding designs analyzed and compared in our numerical investigations. The fiber parameters considered in our calculations are similar to those reported in [36,37]. The HC-AR fibers have a core diameter of 30.5 μm (D_c), a silica wall thickness of t = 1120 nm, and a gap separation g = 6.50 μm. The core diameter is defined as the maximum diameter of a circle that can be inscribed inside the core. It is important to mention that the wall thickness was chosen to give a third AR transmission band centered at around 1.55 μm. A typical nested HC-AR fiber [5,6,11] with 6 circular anti-resonant tubes of diameter D and inner tubes of equal thickness of diameter d is presented in Fig. 1(a). Figure 1(b) depicts a modified form of nested HC-AR fiber in which a supporting solid silica rod joins the inner and outer anti-resonant cladding tubes. Figure 1(c) shows an HC-AR fiber with a straight glass bar at the center of the cladding tubes. Finally, a conjoined HC-AR fiber is presented in Fig. 1(d) [36,37]. The outer tubes are separated by a gap distance, g forming a node-free core boundary [6]. The node-free configuration provides better loss properties and flatter transmission spectra compared to closed core boundary structures [6]. In all of our numerical investigations, we used a small penetration of t/2 of (i) all cladding tubes into the outer jacket tube and (ii) smaller nested tubes into the outer tubes, in order to achieve our simulations closer to the real case according to [39].

3. Numerical results

To perform the numerical calculations, we used a finite-element method COMSOL mode solver. In order to accurately model the leakage loss of the fiber, we used perfectly-matched layers (PML) outside the fiber domain, and both mesh size and PML parameters were optimized according to prior studies [6,11,43,45]. We found that mesh sizes in the thin silica walls are critical in order to achieve accurate results. Extremely fine mesh sizes of λ/4 and λ/6 in air and in the silica walls were used [6]. The choice of such mesh sizes give excellent agreement with the experimental results [6,46]. To ensure convergence of the numerical results, the code was tested by reproducing the results of [5,6].

3.1 HC-AR fibers with six anti-resonant tubes

We first consider the HC-AR fibers with six anti-resonant tubes. The calculated loss spectra and near-field profiles of the fundamental modes for the four fiber designs are presented in Fig. 2. In these calculations, the power overlap with the silica struts was used to estimate the effective material loss. Material loss was then added to the leakage loss and SSL in order to obtain the total propagation loss. The SSL arises from imperfections of the fiber which result in light scattering from the air-glass interfaces. However, HC-AR fibers exhibit low SSL as compared to HC-PBG because the field intensities at the air-glass interfaces are relatively low [6]. The SSL was calculated accordingly to the method reported in [6]. The solid red line shows the propagation loss of a regular nested HC-AR fiber with a loss level of ~0.95 dB/km at 1.55 μm. As a comparison, we also calculated the loss of a typical HC-AR fiber without nested tubes (not shown here) obtaining a total propagation loss of ~130 dB/km at 1.55 μm. The solid blue line is the propagation loss of the modified nested HC-AR fiber with one supporting rod. In this case the propagation loss is ~2 dB/km at 1.55 μm. The solid green line corresponds to the D-shaped HC-AR fiber with ~2.5 dB/km loss at 1.55 μm. Finally, the solid black line depicts the loss spectrum of the conjoined HC-AR fiber with a loss value of ~2 dB/km at 1.55 μm. In general, the regular nested HC-AR fiber has slightly lower loss and smoother transmission spectra than the other cladding structures. The modified nested fiber displays a very similar loss curve (blue). On the other hand, a series of loss peaks appear in the conjoined HC-AR fiber and D-shaped HC-AR fibers. This is due to the fact that they have two glass nodes close to the core boundary giving rise to additional Fano resonances [36].

Optics EXPRESS

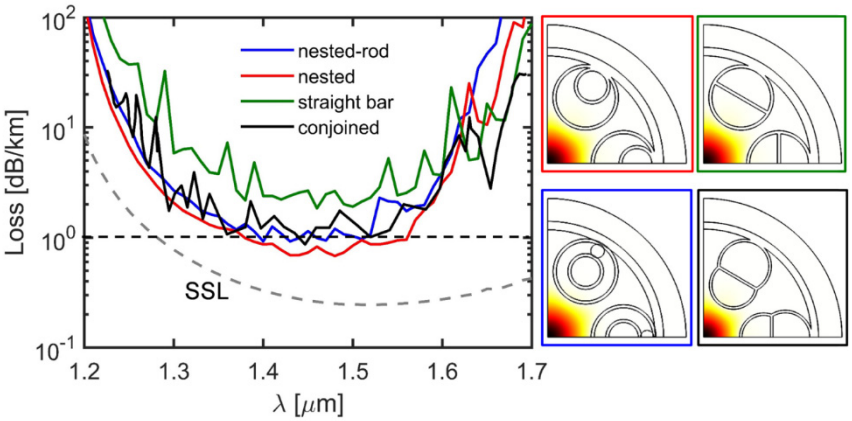

Fig. 2. Calculated propagation loss spectra of different 6-tube HC-AR fibers. All structures have the same core diameter, D_c = 30.5 μm and uniform silica strut thickness, t = 1120 nm. The color of the frame corresponds to the color of the line in the plot. The gray broken line indicates SSL.

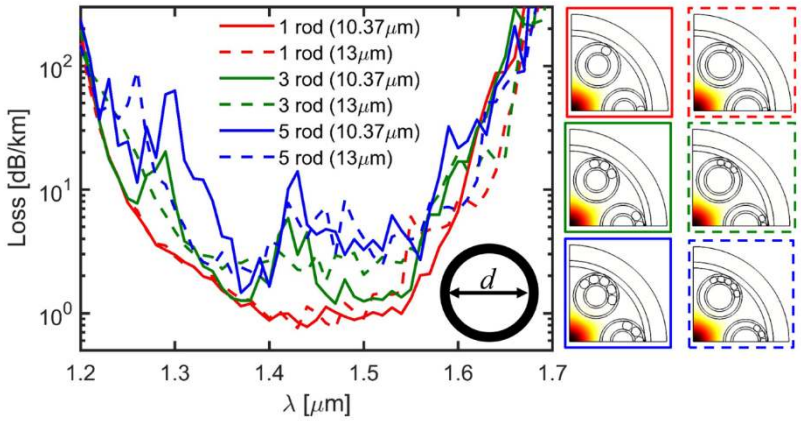

Fig. 3. Calculated propagation loss spectra of 6-tube nested HC-AR fiber with different numbers of solid silica rods and different smaller tube diameters (d). All structures have the same core diameter D_c = 30.5 μm and a uniform silica strut thickness t = 1120 nm. The color of the frame corresponds to the color of the line in the plot. The solid lines and broken lines show the loss spectra for d = 10.37 μm and 13 μm, respectively.

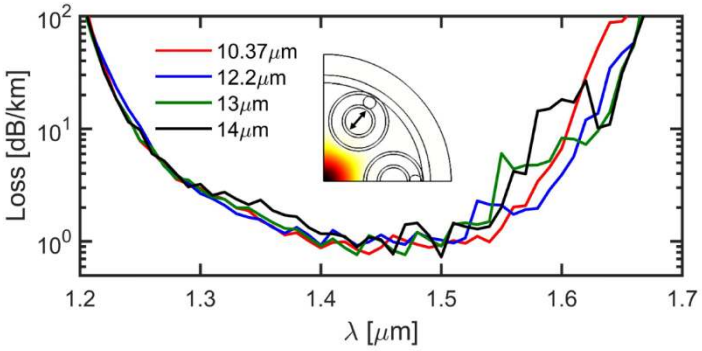

Fig. 4. Calculated propagation loss spectra of 6-tube nested HC-AR fiber with 1 solid supporting rod and different smaller tube diameters (d). All structures have the same core diameter D_c = 30.5 μm and a uniform silica strut thickness t = 1120 nm.

Optics EXPRESS

In another set of simulations, we investigated the dependence of the loss on the number of supporting rods in our modified nested HC-AR fiber. These studies were conducted for fibers with one, three, and five supporting rods and two inner tube dimensions (d = 10.37 μm and d = 13 μm). These results are presented in Fig. 3. As demonstrated in this figure, regardless of the inner tube diameter, increasing the number of supporting rods degrades the transmission characteristics of the fibers. Additionally, fibers with three and five rods display more pronounced loss peaks. To make sure that the loss of the modified nested fiber is not sensitive to the dimension of the inner tube, we scanned the size of the inner anti-resonant tube from (10.37 μm to 14 μm). As it can be seen from Fig. 4, the loss spectrum slightly changes in the shorter wavelength regime as d changes, however the loss effect is more pronounced in the longer wavelength regime. From a fiber manufacturing perspective, this observation is important as it relaxes some fabrication constraints for such fibers.

3.2 HC-AR fibers with five anti-resonant tubes

Next, we extend our investigations to HC-AR fibers with five anti-resonant cladding tubes. It is worth mentioning that most of the previous HC-AR fiber studies have considered fibers with 6 or more anti-resonant cladding tubes [4–6,38,45]. Only recently, a few numerical works have presented 5-tube fiber designs [36]. Figure 5 displays the calculated loss spectra for the nested, modified nested and conjoined 5-tube fiber geometries. In this figure, the green solid line corresponds to the nested HC-AR fiber with a minimum loss value ~0.5 dB/km. Red and blue lines are for the modified HC-AR fibers with one and two supporting rods showing minimum propagation losses of 0.5 dB/km and ~0.65 dB/km, respectively. As demonstrated in this figure, comparable loss spectra are obtained for the nested and modified nested fibers. Moreover, these 5-tube fibers have lower loss values and wider transmission bands than their 6-tube equivalents with same core diameters shown in Fig. 2. As it can be seen from Fig. 5, the calculated minimum loss of the conjoined HC-AR fiber (black) is ~2 dB/km. The larger loss in this fiber is not unexpected as between the anti-resonant walls there are larger air-regions, which can support modes with equal or slightly larger effective mode index than the core mode. This results in a higher loss for the fundamental like mode [6]. The loss can be improved by adding extra anti-resonant bars which in turn reduce the dimensions of the air-regions [36]. Moreover, in this fiber, large Fano-induced loss oscillation are apparent across the transmission band.

3.3 Higher order mode extinction ratio

In order to better understand the modal contents of HC-AR fibers, we show contour plots of the FM and HOMs propagation loss as a function of normalized tube diameter (D/D_c) and normalized nested tube diameter (d/D) for a 5-tube nested fiber in Fig. 6. From these maps it is possible to identify design regions for low loss and effectively single-mode operation. It is evident from Fig. 6(b) that the FM loss remains <1 dB/km in the range of $0.7< D/D_c <1.15$ and $0.5< d/D<0.7$. For a normalized tube diameter, $D/D_c<0.68$, the FM mode loss progressively increases with decreasing values of d/D. Figure. 6(c) shows the loss of HOMs (lowest loss among the LP_{11} and LP_{21} modes). The HOM loss can be made as high as 6000 dB/km for $D/D_c \simeq 1.129$ and $d/D \simeq 0.675$ while maintaining the FM loss below 0.5 dB/km. This large loss value of HOMs is due to the strong coupling between HOMs and cladding modes [6,43,45]. Our results indicate that HOMs can be strongly suppressed by properly engineering the anti-resonant cladding structure. In addition, Fig. 6(d) shows the calculated higher-order mode extinction ratio (HOMER), which is defined as the ratio between the propagation loss of the HOM with the lowest loss and the propagation loss of FM [6,43]. For $D/D_c \simeq 1.129$ and $d/D \simeq 0.675$, the HOMER is >12000. To the best of our knowledge, this is the highest reported HOMER value in any HC-AR fiber.

Optics EXPRESS

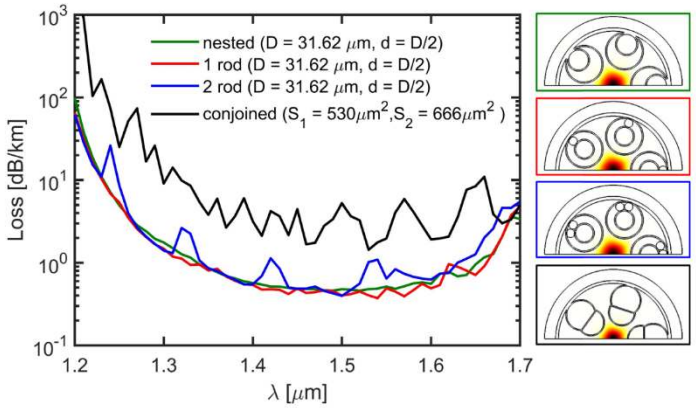

Fig. 5. Calculated propagation loss spectra of different 5-tube HC-AR fibers. All fibers have the same core diameter D_c = 30.5 μm and a uniform silica strut thickness t = 1120 nm. The color of the frame corresponds to the color of the line in the plot.

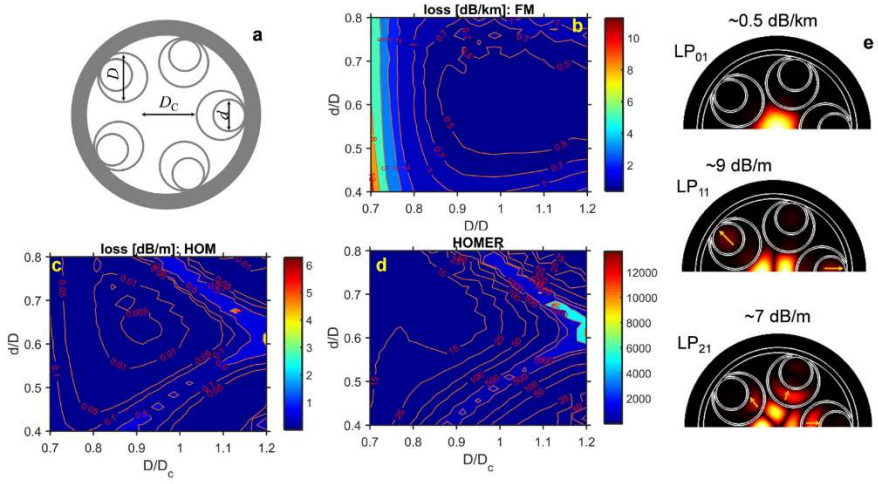

Fig. 6. (a) Geometry of a nested HC-AR fiber with five anti-resonant tubes. Calculated total propagation loss of (b) LP_{01}-like FM and (c) HOMs. (d) HOMER as a function of d/D with different values of D/D_c. (e) Mode field profile of LP_{01}, LP_{11}, and LP_{21} at $D/D_c \simeq 1.05$ and $d/D \simeq 0.68$. The light leakage into the cladding for HOMs are indicated by arrows. HOM loss in (c) is defined as the lowest loss among the four LP modes (LP_{11}^a, LP_{11}^b, LP_{21}^a, and LP_{21}^b). All simulations are performed at 1.55 μm. The fiber has a fixed core diameter D_c = 30.5 μm and a uniform silica strut thickness t = 1120 nm.

To further understand the underlying coupling mechanism between HOMs and cladding modes, we performed simulations with fixed core diameter D_c and fixed tube diameter D, while we vary the inner tube diameter d. Figure 7 shows the effective mode index, propagation loss of the first five core-guided modes (LP_{01}, LP_{11}^a, LP_{11}^b, LP_{21}^a, and LP_{21}^b), and HOMER as a function of d/D from 0.25 to 0.65. From this figure, it is evident that for all modes, the effective mode indices remain almost constant as d/D changes. In other words, the propagation constants do not change because of the fixed core size.

Optics EXPRESS

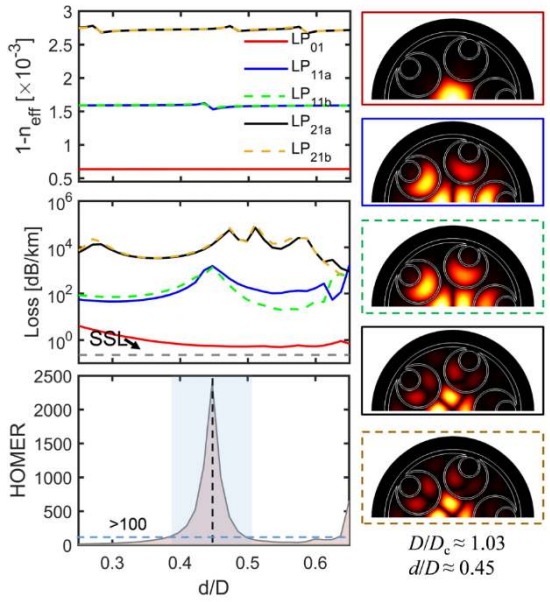

Fig. 7. Effect of changing the inner tube diameter d while the core diameter D_c = 30.5 μm, the strut thickness t = 1120 nm, and the tube diameter D = 31.62 μm remain constant. The simulations are performed at 1.55 μm. Mode field profiles of the first core guided modes are shown at the right hand side for $D/D_c \simeq 1.03$ and $d/D \simeq 0.45$. The color of the frame corresponds to the color of line of the plot.

Interestingly, the FM loss remains ~1dB/km over a wide range of d/D values, whereas the HOMs loss strongly depends on d/D. The largest HOMER is obtained for $d/D \simeq 0.45$, where strong coupling between the HOMs and cladding modes can occur. As a comparison, similar calculations are carried out for a 6-tube HC-AR fiber, see Fig. 8. Here, the loss of the FM mode can also be <1 dB/km within a narrower range of d/D and D/D_c as compared to that of the 5-tube fiber (Fig. 6). This is expected because in the 6-tube fiber, both the distance between the core and outer tube and the separation between the nested and the outer tubes are smaller compared to 5-tube structures. The maximum HOMs loss is obtained when D/D_c is large. However, this requires a small separation between the outer anti-resonant tubes forming core boundary -a requirement that might lead to challenges in the fabrication process. A HOMER maximum of ~200 is obtained, a value far lower than in 5-tube HC-AR fiber.

Finally, we also investigate the loss and HOMER properties of a modified HC-AR fiber as a function of D/D_c and d/D. The results are illustrated in Fig. 9. The FM loss remains < 1 dB/km over a wide range of D/D_c with a minimum loss of ~0.3 dB/km. Importantly, we observe that the FM loss does not change over a wide range of d/D and D/D_c values. In other words, the results indicate that both the outer and nested anti-resonant tubes do not need to be inflated much in order to keep loss levels of the FM below 1 dB/km. We believe that this is advantageous in terms of fabrication. However, the HOMER in this modified nested fiber can only be made slightly higher than 25, because the coupling effect between the HOMs and cladding modes are relatively weak.

3.4 Effect of tube number on propagation loss

In this section we study the effect of the number of anti-resonant tubes on the propagation loss for regular and modified nested HC-AR fiber. We first directly compare regular nested HC-AR fibers with five, six and seven tubes, see Fig. 10. These results clearly indicate that the 5- tube HC-AR fiber shows improved loss performance (lower loss and broader

Optics EXPRESS

transmission window) compared to 6 and 7-tube fibers. Figure 10(a) illustrates that the total loss for the 5-tube structure is ~0.5 dB/km at 1.55 μm and the minimum loss is 0.45 dB/km at 1.49 μm. Similarly, for our modified nested HC-AR fiber with one supporting rod, the 5-tube fiber presents the lowest loss and widest low loss band (Fig. 10(b)). The lower loss and broader transmission window of this fiber is due to its larger distance between the core surround and the outer tube compared to the 6 and 7-tube fibers.

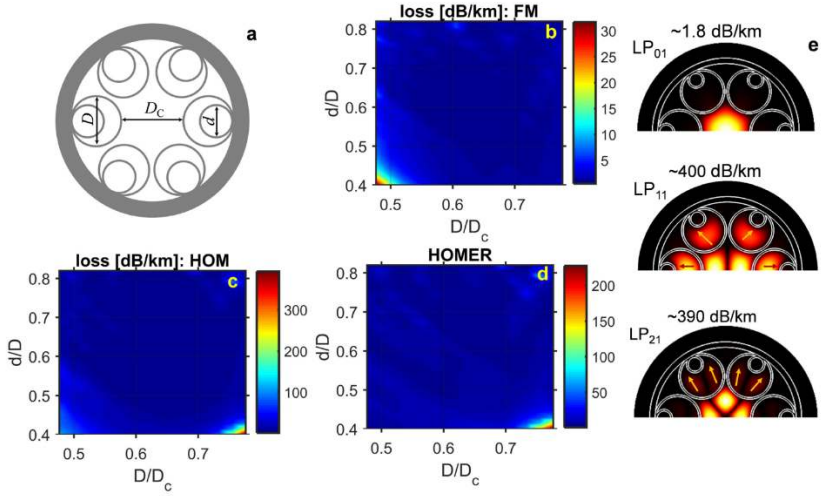

Fig. 8. (a) Geometry of a nested HC-AR fiber with six anti-resonant tubes. Calculated total propagation loss of (b) LP_{01}-like FM and (c) HOMs. (d) HOMER as a function of d/D for different values of D/D_c. (e) Mode field profiles of LP_{01}, LP_{11}, and LP_{21} at $D/D_c \simeq 0.77$ and $d/D \simeq 0.4$. The light leakage into the cladding for HOMs is indicated by arrows. HOM loss in (c) is defined as the lowest loss among the four LP modes (LP_{11}^a, LP_{11}^b, LP_{21}^a, and LP_{21}^b). All simulations are performed at 1.55 μm. The fiber has a fixed core diameter D_c = 30.5 µm and a uniform silica wall thickness t = 1120 nm.

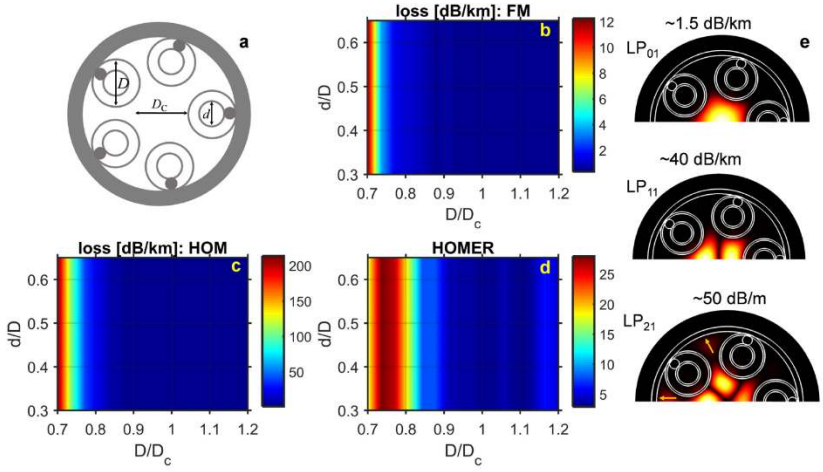

Fig. 9. (a) Geometry of a nested HC-AR fiber with five anti-resonant tubes and one supporting solid rod. Calculated total propagation loss of (b) LP_{01}-like fundamental mode (FM) and (c) higher-order modes (HOMs). (d) HOMER as a function of d/D with different values of D/D_c. (e) Mode field profiles of LP_{01}, LP_{11}, and LP_{21} at $D/D_c \simeq 0.75$ and $d/D \simeq 0.5$. The light leakage into the cladding for HOMs is indicated by arrows. HOM loss in (c) is defined as the lowest loss among the four LP modes (LP_{11}^a, LP_{11}^b, LP_{21}^a, and LP_{21}^b). The simulations are performed at 1.55 μm.

Optics EXPRESS

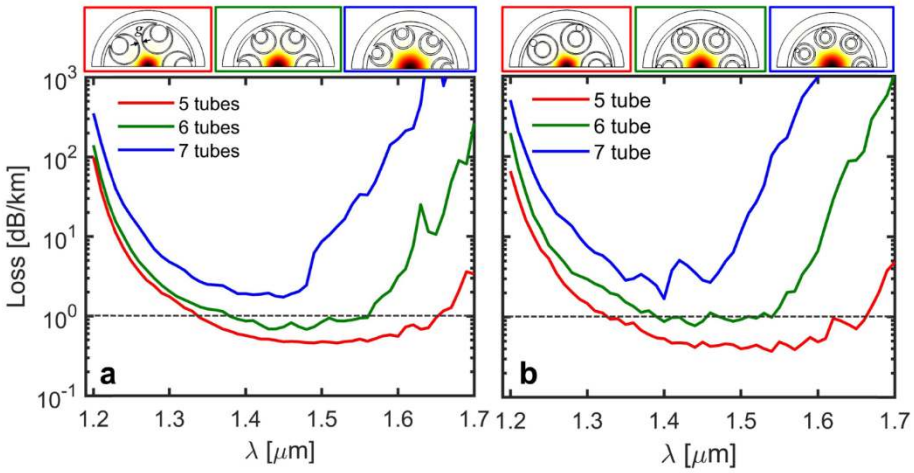

Fig. 10. Calculated loss spectra of regular (a) and modified (b) nested HC-AR fibers with five, six, and seven tubes. All fibers have the same core diameter D_c = 30.5 μm, a uniform silica strut thickness t = 1120 nm, and same gap distance g. The color of the frame corresponds to the color of line of the plot.

We also investigated that choosing HC-AR fiber with less than five tubes increases FM losses. For example, four tube designs with the same core diameter, silica wall thickness, and tube separation exhibit high propagation losses of ~4.5 dB/km at 1.55 μm. Naturally, the size of the air-regions inside the tubes increases with a decrease in the number of tubes. Very large air-regions in few-tube designs can result in modes with equal or even higher refractive index than the core boundary leading to high FM losses [6] as well as high bend losses.

3.5 Bend loss

In this section, we discuss the bend loss of different 5-tube HC-AR fibers. The bend loss was calculated following the approach in [6]: $n_b = n(x,y)e^{(x/R_b)}$, where R_b is the bend radius, x is the bend direction, $n(x, y)$ is the refractive index profile of the straight fiber and n_b is the equivalent refractive index after bending. Figure 11 depicts the calculated bend loss vs. bend radius. For the regular nested HC-AR fiber (green curve), the bend loss remains below 1 dB/km for bend radii larger than 5 cm. The sharp peak observed at around 2 cm bend radius is due to an anti-crossing between the core and cladding modes, as indicated by the calculated mode field profile on the right hand side. The bend loss of the conjoined HC-AR fiber (black curve) is approximately 10 times higher compared to the other fiber designs. This is due to the larger air-regions in the cladding structure which, in turn, facilitate coupling between the core and cladding modes. On the other hand, the modified nested capillary fibers with one and two supporting rods (red and blue curve, respectively) show better bend loss performance. Moreover, the modified nested fiber with 1 supporting rod has the lowest bend loss among all the studied structures. In this fiber, the bend loss is < 1 dB/km for R_b > 3 cm.

Optics EXPRESS

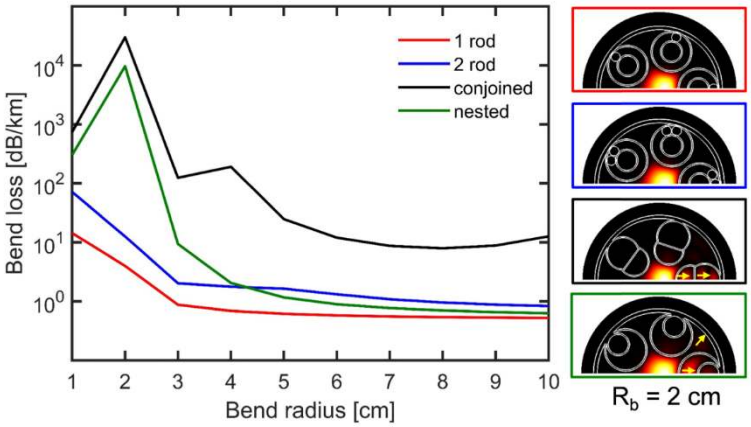

Fig. 11. Calculated bend loss vs. bend radius at 1.55 μm. All fibers have the same core diameter D_c = 30.5 µm and the same gap distance g. The silica strut thickness is t = 1120 nm. Fundamental mode field profiles for a bend radius of 2 cm are shown on the right. The colors of the frames on the right correspond to the line colors in the plot on the left.

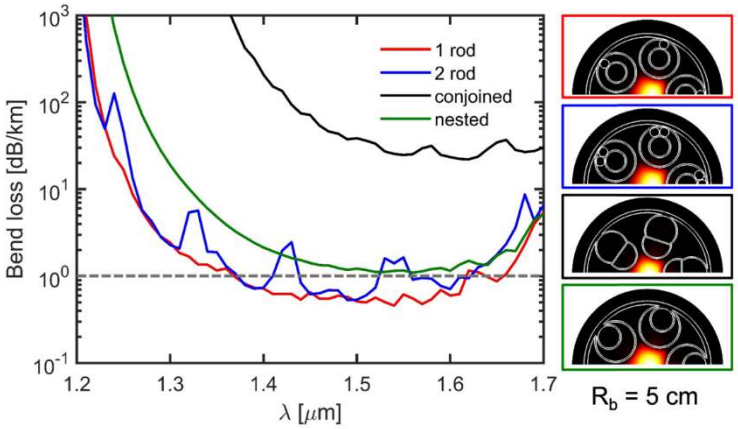

Fig. 12. Calculated wavelength dependent bend loss for a 5 cm bend radius. All fibers have the same core diameter D_c = 30.5 µm, silica strut thickness t = 1120 nm, and gap distance, g. The calculated fundamental mode field profile is shown on the right column. The colors of the frames on the right correspond to the line colors in the plot on the left.

Figure 12 shows the wavelength dependent bend loss for the 5-tube HC-AR fibers calculated for 5 cm bend radius. Here, the modified HC-AR fiber with 1 supporting rod has again the lowest loss over the full transmission band and remains below 1 dB/km from ~1.38 μm to 1.62 μm. Among the studied design, the conjoined HC-AR fiber exhibits the highest loss (20 dB/km at 1.55 μm).

4. Conclusion

In summary, we have investigated various HC-AR fibers and identified designs for low propagation loss <1 dB/km, low bend loss, and effectively single-mode operation in the telecommunication window. In order to get full information about the modal contents of the fibers, we analyzed and optimized the loss and single-mode properties by carefully varying the normalized tube diameter (D/D_c) and the normalized nested tube diameter (d/D). We demonstrate that details of the cladding structure and the number of anti-resonant cladding tubes significantly affects the propagation loss and single-mode operation. We presented new 5-tube nested HC-AR fiber designs with wider transmission bandwidth and lower propagation

loss than equivalent 6 (or more) anti-resonant cladding tubes. We found that strong suppression of HOMs is achieved for 5-tube fibers. In particular, the 5-tube nested HC-AR fiber has a HOMER ~12000 whereas 6-tube fibers have a maximum HOMER of ~200. Moreover, we presented a modified nested capillary HC-AR fiber design with supporting rods between the outer and inner anti-resonant cladding tubes. We found that the propagation loss can be as low as 0.35 dB/km at 1540 nm while remaining below 1 dB/km for a large wavelength range from 1330 to 1660 nm. Significantly, we observed that in the 5-tube HC-AR fiber designs the FM loss remains below 1 dB/km over a much wider range of cladding parameters compared to the 6-tube HC-AR fiber. In other words, the loss does not change much with nested tube parameter variations which provides some fabrication flexibility. We believe that this will reduce the fabrication difficulties and lead to a fiber design that can be more easily realized. Finally, these 5-tube HC-AR fibers show low bend loss even under tight bend conditions and can be coiled to a few cm bend radius.

Funding

Army Research Office (ARO) (W911NF-17-1-0501 and W911NF-12-1-0450); Joint Technology Office High Energy Laser (JTO-HEL) (W911NF-12-1-0450); Air Force Office of Scientific Research (AFOSR) FA9550-15-10041); Danish Research Council (4184-00359B and 8022-00091B).

References

1. R. F. Cregan, B. J. Mangan, J. C. Knight, T. A. Birks, P. S. J. Russell, P. J. Roberts, and D. C. Allan, "Single-Mode Photonic Band Gap Guidance of Light in Air," Science **285**(5433), 1537–1539 (1999).
2. J. C. Knight, J. Broeng, T. A. Birks, and P. S. J. Russell, "Photonic Band Gap Guidance in Optical Fibers," Science **282**(5393), 1476–1478 (1998).
3. F. Benabid, J. C. Knight, G. Antonopoulos, and P. S. J. Russell, "Stimulated Raman Scattering in Hydrogen-Filled Hollow-Core Photonic Crystal Fiber," Science **298**(5592), 399–402 (2002).
4. A. D. Pryamikov, A. S. Biriukov, A. F. Kosolapov, V. G. Plotnichenko, S. L. Semjonov, and E. M. Dianov, "Demonstration of a waveguide regime for a silica hollow--core microstructured optical fiber with a negative curvature of the core boundary in the spectral region > 3.5 μm," Opt. Express **19**(2), 1441–1448 (2011).
5. W. Belardi and J. C. Knight, "Hollow antiresonant fibers with reduced attenuation," Opt. Lett. **39**(7), 1853–1856 (2014).
6. F. Poletti, "Nested antiresonant nodeless hollow core fiber," Opt. Express **22**(20), 23807–23828 (2014).
7. are C. Wei, R. Joseph Weiblen, C. R. Menyuk, and J. Hu, "Negative curvature fibers," Adv. Opt. Photonics **9**(3), 504–561 (2017).
8. F. Yu and J. C. Knight, "Negative curvature hollow-core optical fiber," IEEE J. Sel. Top. Quantum Electron. **22**(2), 146–155 (2016).
9. M. I. Hasan, N. Akhmediev, and W. Chang, "Positive and negative curvatures nested in an antiresonant hollow-core fiber," Opt. Lett. **42**(4), 703–706 (2017).
10. A. N. Kolyadin, A. F. Kosolapov, A. D. Pryamikov, A. S. Biriukov, V. G. Plotnichenko, and E. M. Dianov, "Light transmission in negative curvature hollow core fiber in extremely high material loss region," Opt. Express **21**(8), 9514–9519 (2013).
11. M. S. Habib, O. Bang, and M. Bache, "Low-loss hollow-core silica fibers with adjacent nested anti-resonant tubes," Opt. Express **23**(13), 17394–17406 (2015).
12. G. Humbert, J. Knight, G. Bouwmans, P. Russell, D. Williams, P. Roberts, and B. Mangan, "Hollow core photonic crystal fibers for beam delivery," Opt. Express **12**(8), 1477–1484 (2004).
13. F. Gèrôme, P. Dupriez, J. Clowes, J. C. Knight, and W. J. Wadsworth, "High power tunable femtosecond soliton source using hollow-core photonic bandgap fiber, and its use for frequency doubling," Opt. Express **16**(4), 2381–2386 (2008).
14. F. Gérôme, K. Cook, A. K. George, W. J. Wadsworth, and J. C. Knight, "Delivery of sub-100fs pulses through 8m of hollow-core fiber using soliton compression," Opt. Express **15**(12), 7126–7131 (2007).
15. A. Urich, R. R. J. Maier, F. Yu, J. C. Knight, D. P. Hand, and J. D. Shephard, "Flexible delivery of Er:YAG radiation at 2.94 μm with negative curvature silica glass fibers: a new solution for minimally invasive surgical procedures," Biomed. Opt. Express **4**(2), 193–205 (2013).
16. J. Anthony, R. Leonhardt, S. G. Leon-Saval, and A. Argyros, "THz propagation in kagome hollow-core microstructured fibers," Opt. Express **19**(19), 18470–18478 (2011).
17. : J. C. Travers, W. Chang, J. Nold, N. Y. Joly, and P. St. J. Russell, "Ultrafast nonlinear optics in gas-filled hollow-core photonic crystal fibers [Invited]," J. Opt. Soc. Am. B **28**(12), A11 (2011).
18. M. Selim Habib, C. Markos, O. Bang, and M. Bache, "Soliton-plasma nonlinear dynamics in mid-IR gas-filled hollow-core fibers," Opt. Lett. **42**(11), 2232–2235 (2017).

19. T. Balciunas, C. Fourcade-Dutin, G. Fan, T. Witting, A. A. Voronin, A. M. Zheltikov, F. Gerome, G. G. Paulus, A. Baltuska, and F. Benabid, "A strong-field driver in the single-cycle regime based on self-compression in a kagome fibre," Nat. Commun. **6**(1), 6117 (2015).
20. P. S. J. Russell, P. Hölzer, W. Chang, A. Abdolvand, and J. C. Travers, "Hollow-core photonic crystal fibres for gas-based nonlinear optics," Nat. Photonics **8**, nphoton.2013.312 (2014).
21. A. I. Adamu, M. S. Habib, C. R. Petersen, J. E. Antonio-Lopez, B. Zhou, A. Schülzgen, R. Amezcua-Correa, O. Bang, and C. Markos, "Deep-UV to mid-IR supercontinuum generation driven by mid-IR ultrashort pulses in a gas-filled fiber," ArXiv180503118 Phys. (2018).
22. A. I. Adamu, M. S. Habib, C. R. Petersen, B. Zhou, A. Schülzgen, J. E. Antonio-Lopez, R. Amezcua-Correa, O. Bang, and C. Markos, "Supercontinuum generation from deep-UV to mid-IR in a noble gas-filled fiber pumped with ultrashort mid-IR pulses," in *Advanced Photonics 2018 (BGPP, IPR, NP, NOMA, Sensors, Networks, SPPCom, SOF) (2018), Paper JTu6E.2* (Optical Society of America, 2018), p. JTu6E.2.
23. M. S. Habib, C. Markos, J. E. Antonio-Lopez, R. A. Correa, O. Bang, and M. Bache, "Multi-stage generation of extreme ultraviolet dispersive waves by tapering gas-filled hollow-core anti-resonant fibers," Opt. Express **26**(19), 24357–24371 (2018).
24. M. I. Hasan, N. Akhmediev, and W. Chang, "Mid-infrared supercontinuum generation in supercritical xenon-filled hollow-core negative curvature fibers," Opt. Lett. **41**(21), 5122–5125 (2016).
25. M. I. Hasan, N. Akhmediev, and W. Chang, "Empirical Formulae for Dispersion and Effective Mode Area in Hollow-Core Antiresonant Fibers," J. Lit. Technol. **36**(18), 4060–4065 (2018).
26. B. Mangan, L. Farr, A. Langford, P. J. Roberts, D. P. Williams, F. Couny, M. Lawman, M. Mason, S. Coupland, R. Flea, H. Sabert, T. A. Birks, J. C. Knight, and R. S. J. Philip, "Low loss (1.7 dB/km) hollow core photonic bandgap fiber," in *Optical Fiber Communication Conference (2004), Paper PD24* (Optical Society of America, 2004), p. PD24.
27. R. Amezcua-Correa, F. Gèrôme, S. G. Leon-Saval, N. G. R. Broderick, T. A. Birks, and J. C. Knight, "Control of surface modes in low loss hollow-core photonic bandgap fibers," Opt. Express **16**(2), 1142–1149 (2008).
28. P. J. Roberts, F. Couny, H. Sabert, B. J. Mangan, D. P. Williams, L. Farr, M. W. Mason, A. Tomlinson, T. A. Birks, J. C. Knight, and P. St. J. Russell, "Ultimate low loss of hollow-core photonic crystal fibres," Opt. Express **13**(1), 236 (2005).
29. F. Benabid and P. J. Roberts, "Linear and nonlinear optical properties of hollow core photonic crystal fiber," J. Mod. Opt. **58**(2), 87–124 (2011).
30. F. Couny, F. Benabid, P. J. Roberts, P. S. Light, and M. G. Raymer, "Generation and Photonic Guidance of Multi-Octave Optical-Frequency Combs," Science **318**(5853), 1118–1121 (2007).
31. G. J. Pearce, G. S. Wiederhecker, C. G. Poulton, S. Burger, and P. St. J. Russell, "Models for guidance in kagome-structured hollow-core photonic crystal fibres," Opt. Express **15**(20), 12680 (2007).
32. B. Debord, M. Alharbi, T. Bradley, C. Fourcade-Dutin, Y. Y. Wang, L. Vincetti, F. Gérôme, and F. Benabid, "Hypocycloid-shaped hollow-core photonic crystal fiber Part I: Arc curvature effect on confinement loss," Opt. Express **21**(23), 28597–28608 (2013).
33. M. Alharbi, T. Bradley, B. Debord, C. Fourcade-Dutin, D. Ghosh, L. Vincetti, F. Gérôme, and F. Benabid, "Hypocycloid-shaped hollow-core photonic crystal fiber Part II: Cladding effect on confinement and bend loss," Opt. Express **21**(23), 28609–28616 (2013).
34. Y. Y. Wang, N. V. Wheeler, F. Couny, P. J. Roberts, and F. Benabid, "Low loss broadband transmission in hypocycloid-core Kagome hollow-core photonic crystal fiber," Opt. Lett. **36**(5), 669–671 (2011).
35. N. V. Wheeler, T. D. Bradley, J. R. Hayes, M. A. Gouveia, S. Liang, Y. Chen, S. R. Sandoghchi, S. M. Abokhamis Mousavi, F. Poletti, M. N. Petrovich, and D. J. Richardson, "Low-loss Kagome hollow-core fibers operating from the near- to the mid-IR," Opt. Lett. **42**(13), 2571–2574 (2017).
36. S. F. Gao, Y. Y. Wang, W. Ding, D. L. Jiang, S. Gu, X. Zhang, and P. Wang, "Hollow-core conjoined-tube negative-curvature fibre with ultralow loss," Nat. Commun. **9**(1), 2828 (2018).
37. S.-F. Gao, Y.-Y. Wang, W. Ding, and P. Wang, "Ultralow Loss (2 dB/km) Hollow-Core Conjoined-Tube Negative-Curvature Fiber," in *Advanced Photonics 2018 (BGPP, IPR, NP, NOMA, Sensors, Networks, SPPCom, SOF) (2018), Paper JTu6E.1* (Optical Society of America, 2018), p. JTu6E.1.
38. B. Debord, A. Amsanpally, M. Chafer, A. Baz, M. Maurel, J. M. Blondy, E. Hugonnot, F. Scol, L. Vincetti, F. Gérôme, and F. Benabid, "Ultralow transmission loss in inhibited-coupling guiding hollow fibers," Optica **4**(2), 209–217 (2017).
39. W. Belardi and J. C. Knight, "Hollow antiresonant fibers with low bending loss," Opt. Express **22**(8), 10091–10096 (2014).
40. A. F. Kosolapov, A. D. Pryamikov, A. S. Biriukov, V. S. Shiryaev, M. S. Astapovich, G. E. Snopatin, V. G. Plotnichenko, M. F. Churbanov, and E. M. Dianov, "Demonstration of CO_2-laser power delivery through chalcogenide-glass fiber with negative-curvature hollow core," Opt. Express **19**(25), 25723–25728 (2011).
41. A. V. Newkirk, J. E. Antonio-Lopez, J. Anderson, R. Alvarez-Aguirre, Z. S. Eznaveh, G. Lopez-Galmiche, R. Amezcua-Correa, and A. Schülzgen, "Modal analysis of antiresonant hollow core fibers using S^2 imaging," Opt. Lett. **41**(14), 3277–3280 (2016).
42. F. Yu, W. J. Wadsworth, and J. C. Knight, "Low loss silica hollow core fibers for 3-4 μm spectral region," Opt. Express **20**(10), 11153–11158 (2012).
43. M. S. Habib, O. Bang, and M. Bache, "Low-loss single-mode hollow-core fiber with anisotropic anti-resonant elements," Opt. Express **24**(8), 8429–8436 (2016).

Optics EXPRESS

44. X. Huang, W. Qi, D. Ho, K.-T. Yong, F. Luan, and S. Yoo, "Hollow core anti-resonant fiber with split cladding," Opt. Express **24**(7), 7670–7678 (2016).
45. M. S. Habib, O. Bang, and M. Bache, "Low-loss hollow-core anti-resonant fibers with semi-circular nested tubes," IEEE J. Sel. Top. Quantum Electron. **22**(2), 156–161 (2016).
46. J. R. Hayes, S. R. Sandoghchi, T. D. Bradley, Z. Liu, R. Slavík, M. A. Gouveia, N. V. Wheeler, G. Jasion, Y. Chen, E. N. Fokoua, M. N. Petrovich, D. J. Richardson, and F. Poletti, "Antiresonant Hollow Core Fiber With an Octave Spanning Bandwidth for Short Haul Data Communications," J. Lit. Technol. **35**(3), 437–442 (2017).